M. P. F. Sutcliffe
H. R. Le
R. Ahmed[1]

Department of Engineering,
University of Cambridge,
Trumpington Street,
Cambridge CB2 1PZ, UK

Modeling of Micro-Pit Evolution in Rolling or Strip-Drawing

The micro-plasto-hydrodynamic lubrication (MPHL) model of pit evolution is extended to account for the variation of sliding speed and strain rate in rolling and drawing processes. Results show that all of the following factors are important: pit angle, lubricant viscosity and pressure viscosity coefficient, material yield stress and sliding speed. Theoretical predictions for the change in pit area during the deformation process are well correlated by a non-dimensional group of these parameters. The model agrees reasonably with the measured change in pit volume and area from drawing experiments on cold rolled stainless steel strip containing both artificial and stochastic roughness.
[DOI: 10.1115/1.1352741]

1 Introduction

Surface finish is a major consideration in metal forming processes. A rough surface on the final product is regarded as unfavourable due to its detrimental effect on fatigue strength and corrosion resistance and for aesthetic reasons, as this gives the surface a poor reflectivity. To achieve a good surface finish and low friction, most forming processes operate in the mixed regime of lubrication, where there is both close boundary contact between the tool and work-piece surfaces and pressurised oil filling the valleys. Figure 1 shows a schematic of two alternative lubrication mechanisms in a roll bite under these conditions. At higher speeds, and depending on the lubricant viscosity, hydrodynamic entrainment of oil in the inlet tends to keep the surfaces separated and prevents effective flattening of the asperities on the strip. Several recent papers have considered this mechanism (Sutcliffe and Johnson [1], Sheu and Wilson [2], Lin et al. [3], and Marsault et al. [4]). An important feature of these models is that asperity flattening is related to plastic deformation in the underlying material as described by Sutcliffe [5] or Wilson and Sheu [6]. The hydrodynamic pressure in the lubricant is derived assuming that it flows in continuous channels.

Although the inlet entrainment mechanism is relevant at higher speeds, at lower speeds there is considerable contact between the surfaces and isolated pits develop on the strip surface. Lo [7,8] identifies a ''percolation threshold'' film thickness, below which isolated pits will form. In the presence of sliding between the tool and strip, oil can be drawn out of the pits due to hydrodynamic action, as illustrated schematically in Fig. 1, reducing friction and altering the surface roughness on the work-piece (Mizuno and Okamoto [9], and Kudo and Azushima [10]). This mechanism, which has been described as micro-plasto-hydrodynamic lubrication (MPHL), is the focus of this paper. This behavior is particularly relevant to rolling of stainless steel, where the surface generated after shot-blasting and pickling encourages pit formation. This behavior has also been investigated experimentally by Wang et al. [11], using artificial micro-pits on strip, who find that changes in pit volume and friction correlate with the sliding ratio. Recent observations by Ahmed and Sutcliffe [12] confirm that micro-pits are the dominant features of the surface of cold rolled or drawn stainless steel sheets.

Although micro-pits play an important role in the surface finish of stainless steel, understanding of their evolution during forming processes is very limited. Lo and Wilson [13] propose a theoretical model to investigate this lubrication mechanism, describing the oil pressure variation at the edge of the pit using Reynolds' equation and adopting the effective hardness approach for the asperities introduced by Wilson and Sheu [6]. The change in the asperity flattening rate and the MPHL film thickness can be followed during sliding. A stochastic friction model is applied to derive the friction stress in the contact. The results show that the friction stress depends on the product of the viscosity and sliding speed as observed by Mizuno and Okamoto [9] and Kudo and Azushima [10]. This model does not, however, address the effect of MPHL on the surface finish. Moreover the assumptions of constant bulk strain rate and sliding speed restrict the application of this model to rolling and drawing processes. Sheu et al. [14] examine the details of pit elimination both theoretically and experimentally for larger cavities superimposed on a smaller scale of roughness, concluding that the interaction between these two scales of roughness is important in forging.

The purpose of this paper is to apply the Lo and Wilson MPHL model [13] to strip rolling and drawing processes, in which both the bulk strain rate and the sliding speed vary through the contact. This paper will review the theory and describe its application to rolling and drawing. The theoretical results, including a sensitivity analysis will be presented and compared with experimental measurements of pit evolution during drawing. The relative importance of the mechanisms of lubrication entrainment in the inlet and MPHL in the bite will be discussed.

2 Micro-Plasto-Hydrodynamic Lubrication (MPHL) Model

The MPHL model takes as its starting point the work of Lo and Wilson [13]. A summary of their model and details of any modi-

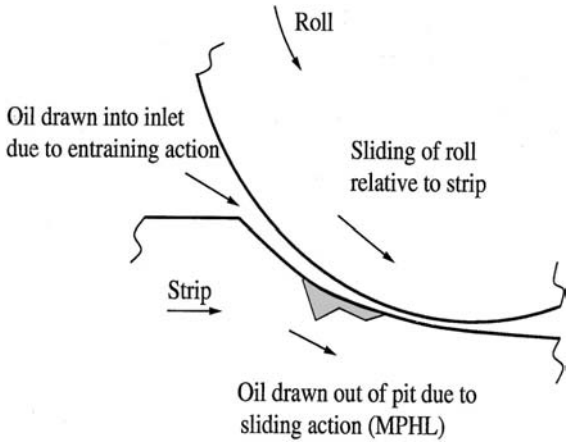

Fig. 1 Schematic of inlet and MPHL lubrication mechanism

[1]Current address: Department of Mechanical and Chemical Engineering, Heriot-Watt University, Riccarton, Edinburgh, EH14 4AS

Contributed by the Tribology Division for publication in the ASME JOURNAL OF TRIBOLOGY. Manuscript received by the Tribology Division June 22, 2000; revised manuscript received December 7, 2000. Associate Editor: B. O. Jacobson.

fications are given in this section. Further details of Lo and Wilson's model are given in the Appendix. The application of the model to rolling and drawing is described in the next section. Lo and Wilson consider the contact between a smooth tool and rough work-piece, modeling the roughness due to pits by a regular row of triangular valleys aligned perpendicularly to the sliding direction, as shown in Fig. 2. It is assumed that the workpiece is first compressed under a uniform pressure $\bar{p}$ to an initial contact ratio A_0. In this process, which is supposed to occur over a short distance at the inlet, the lubricant becomes trapped in the valleys. The geometry at this point is described by the pit angle θ, the spacing between adjacent valleys L_0, and the contact ratio A_0. In the bite itself, oil can be drawn out from the valley due to sliding between tool and workpiece, as shown in Fig. 3. The evolution of the local geometry in this sliding region is the object of the MPHL model. It is assumed that the pit angle θ is unchanged during the deformation process, so that the subsequent pit geometry is described by the area of contact ratio A and pit spacing L.

2.1 Oil Film Thickness at the Pit Edge. By considering volume conservation for the oil and strip material as the pit geometry evolves, Lo and Wilson [13] derive an expression for the oil film thickness h_1 at the trailing edge of the pit as

$$h_1 = -\frac{2\theta L^2(1-A)(\dot{\varepsilon}-A\dot{\varepsilon}_a)}{2u_1+AL\dot{\varepsilon}_a}. \tag{1}$$

$\dot{\varepsilon}$ and $\dot{\varepsilon}_a$ are the bulk strain and asperity flattening rates, and u_1 is the relative sliding velocity between the tool and strip at the trailing edge of the pit. Details are given in the Appendix.

2.2 Hydrodynamic Pressure. The previous section derives an expression for the film thickness h_1 at the edge of the pit based on geometric arguments. An expression for the film thickness can also be derived based on the hydrodynamics. Due to the local wedge action at the trailing edge of the pit, the lubricant pressure builds up there, as shown schematically in Fig. 3. The interface pressure on the plateaux p_p rises above the mean pressure $\bar{p}$ while the valley pressure p_v falls below the mean. The hydrodynamic pressure build-up is derived using the one-dimensional Reynolds' equation

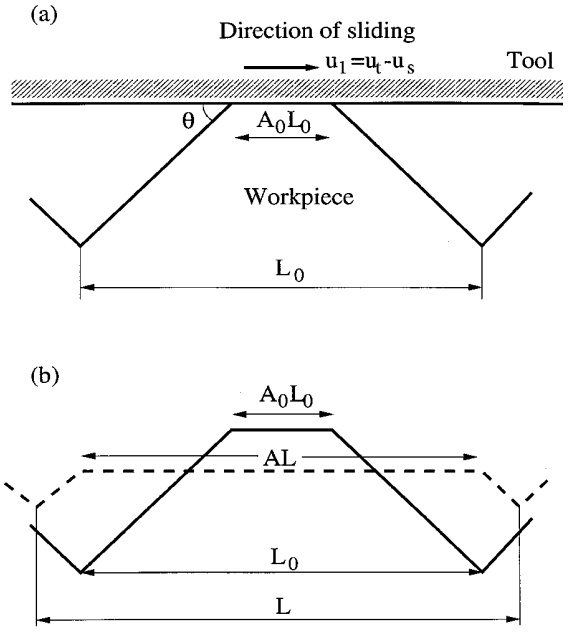

Fig. 2 Schematic of flattening of an asperity: (*a*) initial asperity; (*b*) comparison between deformed and initial asperity, after Lo and Wilson [13].

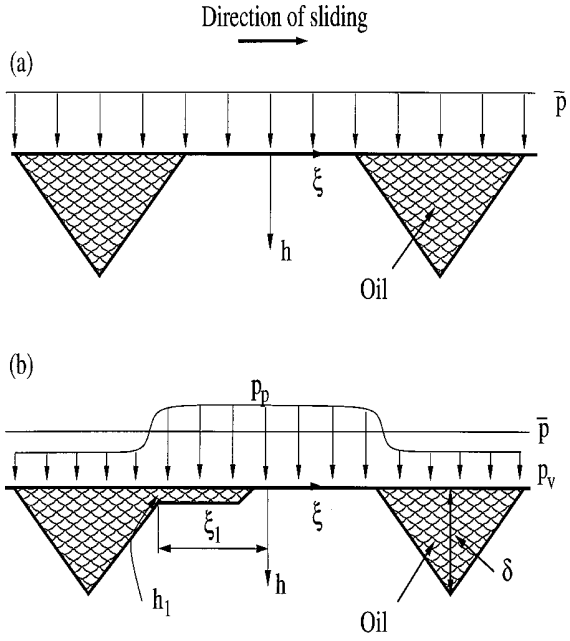

Fig. 3 Schematic of micro-pit evolution due to sliding in the bite: (*a*) isolated micro-pits under uniform contact pressure; (*b*) oil drawn out by sliding, after Lo and Wilson [13].

$$\frac{dQ}{d\xi} = 12\eta_0\alpha\bar{u}_1\frac{h-h^*}{h^3}, \tag{2}$$

where $Q=1-e^{-\alpha p}$ is the reduced pressure, η_0 is the viscosity at ambient pressure, α is the pressure viscosity index, h is the film thickness, and h^* is a constant, equal to the film thickness when the pressure gradient is zero. The local co-ordinate ξ gives the distance in the sliding direction from the center of the asperity. The mean oil velocity at the edge of the pit $\bar{u}_1$ is related to the sliding speed u_1, as detailed in the Appendix, Eq. (*A*-4). The effect of pressure on oil viscosity is taken into account by the Barus equation $\eta=\eta_0 e^{\alpha p}$. Since the pit angle is assumed constant, $dh/d\xi=-\theta$ and (2) becomes

$$\frac{dQ}{dh} = -\frac{12\eta_0\alpha\bar{u}_1}{\theta}\frac{h-h^*}{h^3}. \tag{3}$$

Integrating this equation gives the reduced pressure Q as a function of film thickness h. The oil film thickness is assumed much smaller than the depth of the pits, so well upstream from the trailing edge of the pit where h is very large, the pressure reaches the valley pressure p_v and the reduced pressure $Q=1-e^{-\alpha p}$. It is further assumed that the pressure gradient becomes zero at the edge of the valley, i.e., $h^*=h_1$. Since the reduced pressure at the edge of the valley is given by $Q=1-e^{-\alpha p_p}$, the outflow film thickness h_1 is determined by

$$h_1 = \frac{6\eta_0\alpha\bar{u}_1}{\theta(e^{-\alpha p_v}-e^{-\alpha p_p})}. \tag{4}$$

The asperity pressure p_p and valley pressure p_v are related by the asperity crushing theory outlined in the next section.

2.3 Asperity Crushing. The flattening velocity of the asperity v_f is the difference between the velocities normal to the surface of the plateau and the valley given by differentiating the mean depth of the valley $\bar{\delta}$ with respect to time t

$$v_f = -\frac{d\bar{\delta}}{dt} = -\frac{\theta L(\dot{\varepsilon}-A\dot{\varepsilon}_a)}{4}. \tag{5}$$

Defining a dimensionless flattening rate W as

$$W=\frac{2v_f}{\dot{\varepsilon}L}, \tag{6}$$

where L is the pit spacing. Sutcliffe [15] fits Korzekwa's [16] finite element solution for asperity flattening by the following function of the effective hardness $\Delta=(p_p-p_v)/Y$ and the area of contact ratio A

$$W=A(1-A)(C_1(\Delta)+C_2(\Delta)A+C_3(\Delta)A^2), \tag{7}$$

where the functions $C_1(\Delta)$, $C_2(\Delta)$, and $C_3(\Delta)$ are given explicitly by Sutcliffe [15]. This model of asperity flattening is considered more appropriate to the conditions pertaining in MPHL than the model used by Lo and Wilson [13]. Combining Eqs. (5) and (6) gives

$$W=-\frac{\theta(\dot{\varepsilon}-A\dot{\varepsilon}_a)}{2\dot{\varepsilon}}. \tag{8}$$

For a given bulk strain rate $\dot{\varepsilon}$ and asperity strain rate $\dot{\varepsilon}_a$, the effective hardness Δ can be found using Eqs. (7) and (8). Therefore, the asperity and valley pressures can be solved as

$$p_p=\overline{p}+(1-A)Y\Delta \tag{9}$$

$$p_v=\overline{p}-AY\Delta \tag{10}$$

and substituted into Eq. (4). Since the asperity strain rate $\dot{\varepsilon}_a$ is the only variable in Eqs. (1) and (4), it can be found by standard non-linear solvers. As the film thickness must be positive and much smaller than the depth of the pit, Lo and Wilson [13] derive two bounds to help solve for $\dot{\varepsilon}_a$.

$$h_1>0, \text{ so that } \dot{\varepsilon}_a>\frac{\dot{\varepsilon}}{A} \text{ and } h_1\ll\frac{\theta L(1-A)}{2},$$

$$\text{giving } \dot{\varepsilon}_a\ll\frac{2(u_1L^{-1}+2\dot{\varepsilon})}{3A}.$$

3 Application to Rolling and Drawing Processes

From the theoretical analysis it is seen that the outflow film thickness h_1 and the asperity strain rate $\dot{\varepsilon}_a$ are governed by the bulk strain rate $\dot{\varepsilon}$ and the sliding speed u_1. The variation of these parameters through the bite in rolling and drawing is found from the geometry of the contact.

Rolling. A schematic of the strip rolling processes is shown in Fig. 4(*a*). For clarity, the tool surface is considered rigid and smooth. The strip is reduced in thickness from z_1 to z_2 through the bite by rolls of radius R, giving a reduction in strip thickness r. The variation in strip thickness is given by a circular arc

$$z=z_2+R\phi^2, \tag{11}$$

where $\phi=(b-x)/R$ is the angle between the roll surface and the horizontal, as illustrated in Fig. 4(*a*), x is a co-ordinate in the rolling direction with origin at the beginning of the bite, and the projected length of arc of contact of the bite b is given by: $b=\sqrt{(z_1-z_2)R}$. The strain rate for the bulk deformation can be found from the geometry of contact as

$$\dot{\varepsilon}=\frac{2\phi u_s}{z}, \tag{12}$$

where u_s is the local strip speed. In practice the direction of sliding reverses at the neutral point. However, since the length of the reversed slip region at the exit is relatively small under industrial conditions, in this paper we simplify the problem by assuming that the strip and roll travel at the same speed at the exit (i.e., zero forward slip). The speed of the strip is given by volume conservation as $u_s=z_2u_r/z$, where u_r is the roll speed, so that the sliding speed is given by

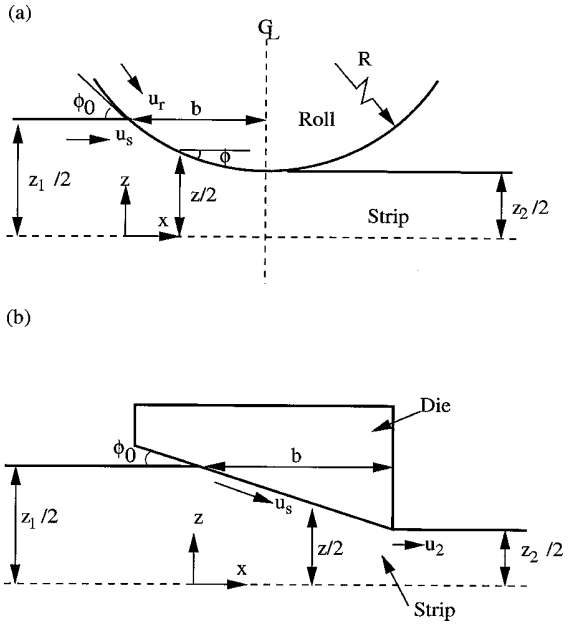

Fig. 4 Schematic of strip forming processes (*a*) rolling and (*b*) drawing

$$u_1=\left(1-\frac{z_2}{z}\right)u_r. \tag{13}$$

Strip Drawing. A schematic diagram of strip drawing as shown in Fig. 4(*b*). The variation in strip thickness through the bite is now given by

$$z=z_1-2x\phi_0, \tag{14}$$

where ϕ_0 is the half die angle. The strain rate is given by

$$\dot{\varepsilon}=\frac{2u_s\phi_0}{z}. \tag{15}$$

The sliding speed is the same as the strip speed in this case and given by

$$u_1=u_s=\frac{z_2u_2}{z}. \tag{16}$$

Implementation in the MPHL Model. In the above sections the variations in bulk strain rate $\dot{\varepsilon}$ and sliding speed u_1 through the bite are derived explicitly. These expressions can be coupled with Eqs. (1) and (4) to give the asperity strain rate $\dot{\varepsilon}_a$. The asperity strain rate $\dot{\varepsilon}_a$ is integrated using a $2^{nd}/3^{rd}$ order Runge-Kutta scheme to give the asperity strain ε_a. The bulk strain ε is calculated explicitly from the thickness of the strip. The variation of the contact ratio, MPHL film thickness and the residual pit volume can then be solved through the bite using the equations detailed in Section 2 and the Appendix.

4 Theoretical Results

This section presents theoretical predictions for rolling and strip drawing. Details of the conditions used in the theoretical calculations are given in Table 1. Rolling conditions are typical of industrial rolling of stainless steel, while drawing conditions are typical of those achievable when drawing stainless steel using the strip drawing rig at Cambridge (Ahmed and Sutcliffe [17]). Strip surface parameters appropriate for cold-rolled stainless steel strip are taken from Ahmed and Sutcliffe [12].

Table 1 Summary of conditions for theoretical calculations

	Rolling	Drawing
Strip entry thickness z_1	4 mm	
Strip reduction r	15 %	
Strip yield stress Y	400–800 MPa	
Initial pit spacing L_0	300 μm	
Pit angle θ	10–20°	
Roll radius R	25 mm	–
Roll speed u_r	1–10 m/s	–
Die semi-angle ϕ_0	–	4°
Strip exit speed u_2	–	0.1–0.001 m/s
Lubricant viscosity η_0	0.007 Pa s	0.15 Pa s
Pressure viscosity coefficient α	1.5×10^{-8} m²/N	2.2×10^{-8} m²/N

4.1 Form of Solution. Figure 5 presents typical results for rolling, showing the predicted variation through the bite of the contact area A and MPHL film thickness h_1 at the edge of the pit for three different rolling speeds. This figure shows how A increases from its initial value of 0.5 as oil is drawn out of the pits in the bite. The film thickness drops quickly at the exit as the sliding speed falls to zero. The film thickness h_1 and contact ratio A both increase with rolling speed as more lubricant is drawn out of the pit, leading to a corresponding reduction in the pit area $(1-A)$. Note that this contrasts with the lubricant entraining mechanism in the inlet to the bite, where an increase in speed tends to draw more oil into the contact, leading to greater trapping of oil in pits, an increase in the pit area and a fall in the area of contact ratio A.

Figure 6 shows the corresponding variation in contact ratio and film thickness through the bite for strip drawing, for a range of drawing speeds. In contrast to the rolling case, there is continued sliding throughout the contact so that the film thickness does not fall to zero at the exit as with rolling. The drop in the MPHL film thickness towards the exit, predicted by Fig. 6, is related to the increase in contact ratio through the bite which inhibits the rate of asperity crushing, c.f. Eq. (7).

4.2 Presentation Using Dimensionless Lubrication Parameters. In this section dimensionless parameters are used to characterize the inlet and MPHL lubrication mechanisms. Results from the MPHL theory are presented as a function of the MPHL

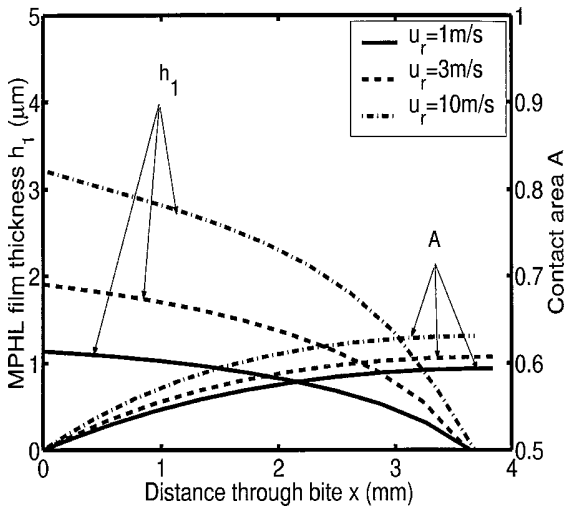

Fig. 5 Theoretical predictions for the variation in trailing edge film thickness h_1 and contact area ratio A through the bite in rolling, $Y=600$ MPa, $A_0=0.5$, and $L_0=300$ μm

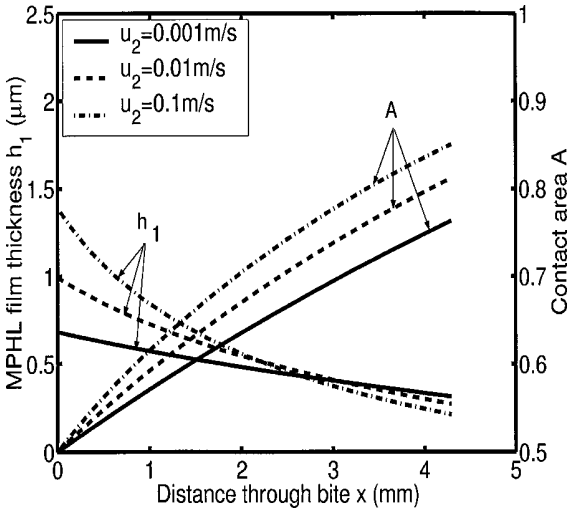

Fig. 6 Theoretical predictions for the variation in trailing edge MPHL film thickness h_1 and contact area ratio A through the bite in strip drawing, $Y=600$ MPa, $A_0=0.5$, and $L_0=300$ μm

lubrication parameter. The relative importance of these mechanisms is identified using a regime map. To characterize lubrication at the inlet to the bite, we use the ratio $\Lambda_i=h_w/\sigma_0$ of the "smooth" film thickness h_w to the combined tool and initial strip roughness σ_0. A film thickness estimate for smooth rolls and strip is given by Wilson and Walowit [18] as

$$h_w=\frac{6\eta_0\alpha\bar{u}}{\phi_0(1-e^{-\alpha Y})}, \tag{17}$$

where $\bar{u}=(u_r+u_{s1})/2$ is the mean entraining velocity at the inlet and ϕ_0 is the inlet angle. Ahmed and Sutcliffe [17] introduced a corresponding parameter Λ_m to characterize MPHL pit lubrication. To make a very approximate estimate of the film thickness at the edge of the pit h_1, they assumed that the lubricant pressures in the pits and on the asperity tops are given by $0.5Y$ and $1.5Y$ respectively. Equation (4) then gives h_1 as

$$h_1=\frac{6\eta_0\Delta u}{\theta(e^{-0.5\alpha Y}-e^{-1.5\alpha Y})}, \tag{18}$$

where Δu is the sliding speed in the inlet and θ is the entraining angle at the edge of the pit. The volume of oil drawn out from the pit, per unit width of pit, as it travels through the bite is estimated by $\Delta\ell h_1/2$, where $\Delta\ell$ is the sliding distance and the factor 2 arises because the mean speed of the film is half the sliding speed. For the triangular pit profiles assumed here, the initial pit volume, per unit width, is equal to $\delta^2/2\theta$, and the ratio Λ_m of the volume of oil drawn out of the pit to the initial pit volume is given by

$$\Lambda_m=\frac{6\eta_0\alpha\Delta u\Delta\ell}{\delta^2(e^{-0.5\alpha Y}-e^{-1.5\alpha Y})}. \tag{19}$$

We expect MPHL effects to be insignificant when Λ_m is small.

For strip drawing the sliding distance $\Delta\ell$ is given by $\Delta\ell=(z_1-z_2)/(2\phi_0)$, while the corresponding expression for rolling can be found by considering the time τ taken for a portion of strip to pass through the bite of length b:

$$\tau=\int_0^b\frac{1}{u_s}dx=\int_0^b\frac{z}{z_2u_r}dx=\frac{b\bar{z}}{z_2u_r}, \tag{20}$$

where $\bar{z}$ is the average thickness with respect to position. In this time the roll has moved a distance τu_r, so that the sliding distance equals

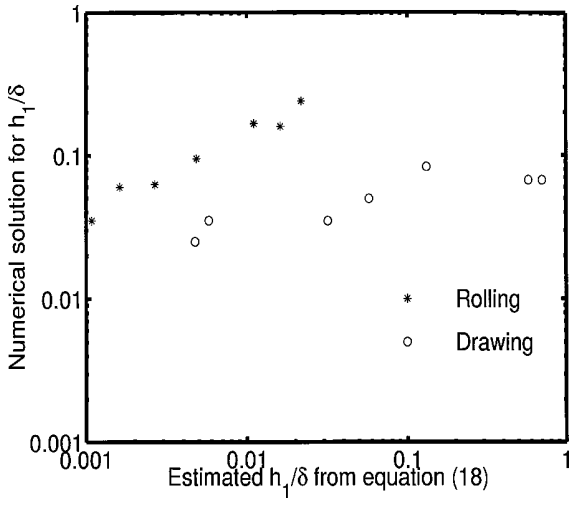

Fig. 7 Correlation between the full numerical prediction and the estimated value from Eq. (18) of the ratio h_1/δ of the trailing edge film thickness to the pit depth

$$\Delta\ell = b\left(\frac{\bar{z}}{z_2} - 1\right). \tag{21}$$

Using the standard quadratic expression for the roll shape, Eq. (11), this becomes

$$\Delta\ell = \frac{b}{3}\left(\frac{z_1}{z_2} - 1\right). \tag{22}$$

To determine the usefulness of the lubrication parameter Λ_m in describing MPHL, a series of additional calculations were performed, in which the yield stress was varied from 400 to 800 MPa and the pit angle was varied from 10 to 20 deg, while the rolling or drawing speed was held at the mid-values quoted in Figs. 5 and 6. The predictions for the initial film thickness h_1 from the full numerical model described in Sections 2 and 3 are compared with Eq. (18) in Fig. 7, for the calculations presented in Figs. 5 and 6 and for these additional calculations. The large difference between the numerical predictions and the estimate of Eq. (18) for the film thickness at the edge of the pit highlight the very approximate nature of this equation.

Figure 8 plots the predicted contact ratio A as a function of Λ_m

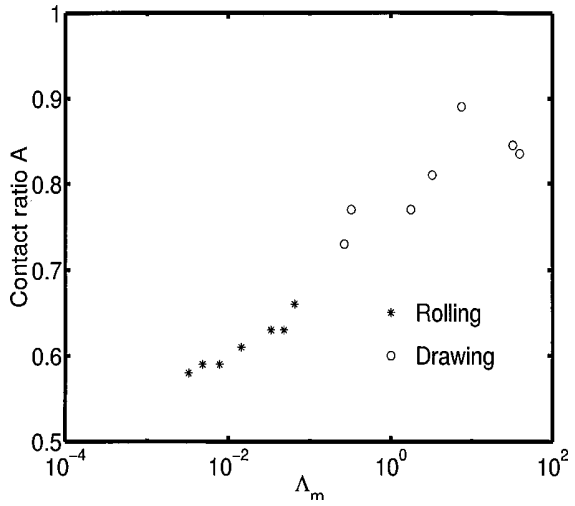

Fig. 8 Variation of contact ratio with Λ_m

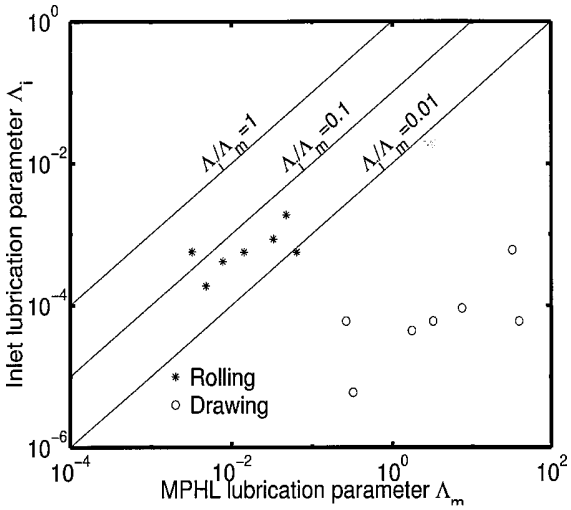

Fig. 9 Lubrication regime map

for these calculations. Notwithstanding the significant difference in film thickness estimate, Fig. 8 shows that Λ_m is indeed a useful parameter to characterize the change in contact ratio A through the bite due to MPHL for both rolling and drawing. Significant elimination of the pits occurs when Λ_m is greater than about 1 as expected.

In Fig. 9, the actual variation in inlet and MPHL parameters Λ_i and Λ_m are plotted on a regime map for the range of parameters considered above, typical of industrial rolling and drawing using the Cambridge rig. In estimating Λ_i we take the r.m.s roughness equal to the pit depth δ. The very low values of inlet film parameter Λ_i for drawing suggest that inlet effects are insignificant in these experiments. However, for rolling it might be expected that interaction between bite inlet and MPHL mechanisms could occur, particular if rolling were done at higher speeds than those currently used (recall that both Λ parameters are proportional to rolling speed).

5 Comparison With Experimental Results

This section compares theoretical predictions of pit evolution with a series of experiments using strip-drawn stainless steel. The first section presents some new experiments using artificial roughness, created using a Vickers indentor, while the second section uses measurements on an as-received rough surfaces described by Ahmed and Sutcliffe [17]. Further details of the drawing set-up and methodology are given in their paper.

Artificial Indentations. To simulate the conditions of the theoretical model, an array of Vickers indentations was generated on bright-annealed 316 stainless steel strips of initial thickness 3 mm, as illustrated in Fig. 10. The pits were much deeper than the strip roughness, and had a slope, in the direction of sliding, of 22 deg. The plane strain yield stress of the strip at typical reductions of 10 percent and 30 percent equals about 770 and 1000 MPa respectively. The exact variation with reduction was taken from proprietary data. The strips were drawn according to the pass schedule of Table 2 at a speed of 0.017 m/s, using flat-faced dies of semi-angle $\phi_0 = 4$ deg, lubricated with Shell Vitrea 68 oil (properties as per the drawing column of Table 1). Table 2 includes the lubrication parameters Λ_m and Λ_i (here the r.m.s. roughness is taken as the depth of the indentations). The pit volume after each pass was estimated from measurements using a Zygo three-dimensional white-light interferometric profilometer. Predictions of the increase in contact area, and corresponding decrease in pit area and volume, were made using the theory described above with the appropriate drawing conditions and pit

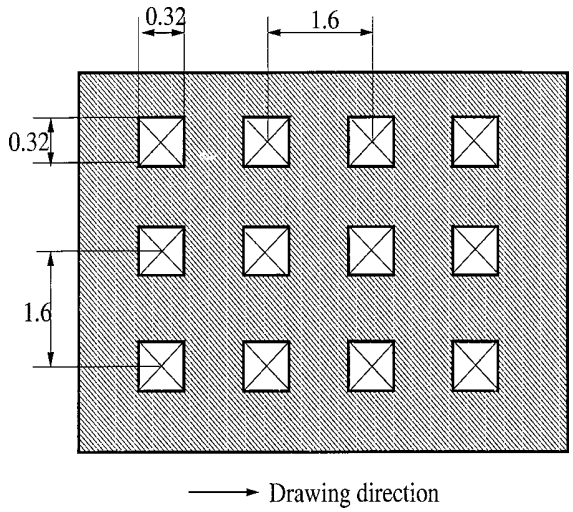

Fig. 10 A schematic of the artificial micro-pits. Dimensions are in mm.

geometry described in this section. Values of $L_0 = 300\ \mu$m and $A_0 = 0.5$ were used for these calculations. An effective yield stress was taken equal to the average for the inlet and exit thicknesses. Figure 11 shows that there is reasonable agreement between the measured and predicted change in pit volume with natural strain.

As-Received Rough Strip. Ahmed and Sutcliffe [17] describe drawing experiments on 316 stainless steel white-hot band. This material had an as-received R_q roughness approximately equal to 7.5 μm and estimated values for pit spacing and slope equal to 300 μm and 15 deg. Experimental details, including die angle, drawing speed and lubricant are as for the previous section. The white-hot band is assumed as perfectly annealed for simplicity, with a variation of yield stress with strain as for the previous section, although Vickers hardness tests indicate that there is some

Table 2 Drawing conditions for strip with artificial micro-pits

Draw no.	Inlet thickness (mm)	Reduction (%)	Λ_i	Λ_m
1	3.0	18	3×10^{-5}	6
2	2.47	12	8×10^{-5}	327

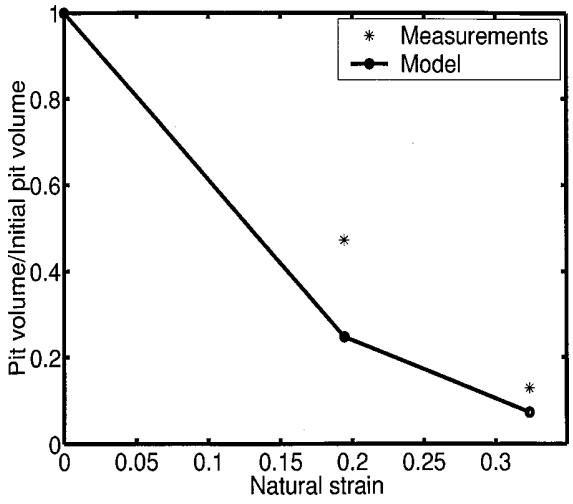

Fig. 11 Comparison between measurements and theory for the change in the volume of the artificial micro-pits during drawing

Table 3 Drawing conditions for white-hot band, from Ahmed and Sutcliffe [17]

Draw no.	Inlet thickness (mm)	Reduction (%)	R_q roughness at inlet (μm)	Λ_i	Λ_m
1	4.1	15.1	7.5	0.0003	80
2	3.48	9.7	3.0	0.0007	1×10^3
3	3.14	9.5	1.3	0.002	$>10^3$

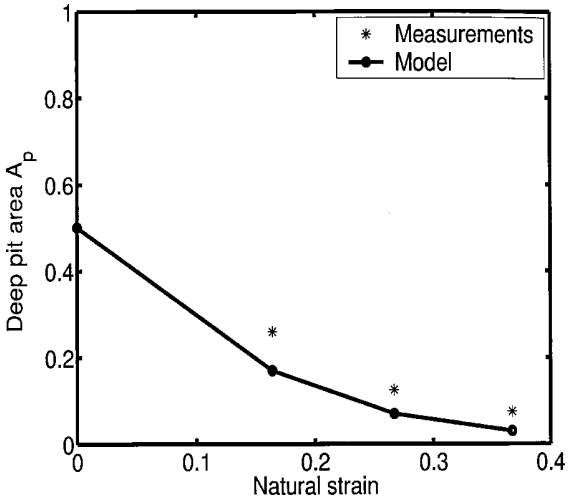

Fig. 12 Comparison between measurements and theory for the change in the pit area of shot-blasted white hot band during drawing

work hardening to the surface associated with the shot-blasting. The pass schedule and values of Λ_m and Λ_i are given in Table 3. Ahmed and Sutcliffe [17] measured the surface roughness of the strip samples with a three-dimensional profilometer and estimated the ''deep pit'' area (actually pits deeper than 0.5 μm) using the method described by Ahmed and Sutcliffe [12]. Theoretical predictions of the change in pit geometry during drawing are made using the appropriate drawing conditions, oil properties and pit geometry as described in this section. Figure 12 shows that, for this random rough surface, again there is reasonable agreement between the measured and predicted change in pit area with natural strain.

6 Application to Industrial Rolling

Although care needs to be taken in applying the work to rolling, this is made much simpler by the use of the dimensionless group Λ_m that automatically allows for differences in lubricant viscosity, sliding distance and speed and rolling speed. Figure 9 suggests that, for the earlier passes considered in these figures and for practical rolling conditions, little oil will be drawn in by entraining action, and little removed by MPHL. The behavior will be dominated by the degree to which oil can be trapped hydrostatically in the inlet and retained in the bite. The role of escape routes for the oil in the bite, associated with roughness on the ''contact'' areas (c.f. [14]), may then become important. Only in the later passes, or at higher speeds than used at present, will the role of the inlet and MPHL mechanisms become important, with significant interaction between these mechanisms. Although Ahmed and Sutcliffe [17] present experimental measurements from rolling, these were taken at the coil ends where the rolling speed is unrepresentative of the bulk of the coil. Further measurements from mid-coil samples and a better understanding of the interaction between the various lubrication mechanisms are needed to gain a fuller under

standing of pit evolution in rolling. Further work also needs to consider in more details the effect of pit geometry. In particular, statistical variations need to be considered, as only the most severe pits are likely to persist towards the end of the pass schedule.

In the work described in this paper, it is assumed that the tool is rigid and smooth, so that there is no wear between the mating surfaces. In many cases, wear is involved and frequently a transfer layer of metal and metal oxides from the rolled strip tends to build up on the tool surface. Preliminary experiments on a drawing rig suggest that this transfer film may enhance the MPHL mechanism and help to eliminate micro-pits. The tool roughness also plays an important role in cold rolling processes. Micro-cutting may occur if rough tools are used, increasing the rate of surface flattening. It has been observed on drawing simulations that micro-pits are eliminated faster using rougher tools, but further work is needed to understand details of these wear mechanisms.

7 Conclusions

The theoretical model of micro-plasto-hydrodynamic lubrication (MPHL) given by Lo and Wilson [13] has been extended to investigate the evolution of micro-pits during strip rolling and drawing. It is assumed that oil is trapped in isolated pits in the inlet and is subsequently drawn out by relative sliding between the tool and workpiece in the bite. The variation of lubricant pressure is modelled using Reynolds' equation and the effect of bulk deformation in the strip is included in modelling the asperity deformation. Theoretical predictions of the oil film thickness at the trailing edge of the pit and the change in pit area through the bite correlate well with the non-dimensional group Λ_m introduced by Ahmed and Sutcliffe [17] to characterize MPHL. Theory predicts that oil is drawn out effectively by MPHL action when Λ_m is greater than about 1, leading to significant elimination of the pits in these circumstances. Predictions of the change in pit volume and area during drawing of stainless steel strip, both for roughness in the form of artificial indents and for the stochastic surface of as-received white-hot band, are in reasonable agreement with experiments.

Acknowledgments

The authors are grateful for the assistance from staff at Avesta Polarit and Corus plc, Swinden Technology Center, in particular Dr. Didier Farrugia, Mr. Peter Freeman, Mr. Gordon Allan, and Mr. Ken King. The financial support of these collaborating companies, the EPSRC and the Newton Trust is gratefully acknowledged.

Nomenclature

$A(A_0)$ = real area of contact ratio between tool and strip (initial area of contact ratio)
$L(L_0)$ = (initial) spacing between pits
Q = reduced pressure, $Q=1-e^{-\alpha p}$
R = roll radius
W = non-dimensional asperity flattening rate
Y = plane strain yield stress of the strip
b = length of the bite
h = lubricant film thickness
h_1 = film thickness generated at trailing edge of pit
h_w = film thickness generated in the inlet
$\overline{p}$ = mean interface pressure
p_p = pressure on the asperity top
p_v = lubricant pressure in the valleys
r = reduction in strip thickness
$\overline{u}$ = mean entraining velocity at inlet to bite
$\overline{u_1}$ = mean velocity of the lubricant at the trailing edge of the pit
u_1 = relative sliding velocity between the roll and strip at the trailing edge of the pit
u_r, u_s = roll and strip speeds
v = volume of the pit, per unit width of strip.
v_f = flattening velocity of the valley
x = co-ordinates in rolling direction, 1-inlet, 2-exit
z = strip thickness, 1-inlet, 2-exit
Λ_i = inlet lubrication parameter: ratio of inlet film thickness to combined tool and strip roughness, $\Lambda_i=h_w/\sigma_0$
Λ_{m} = MPHL lubrication parameter: ratio of an estimate of the volume of oil drawn out of the pit due to micro-plasto-hydrodynamic lubrication to the initial pit volume
Δu = sliding velocity between tool and strip in the bite
$\Delta\ell$ = sliding distance in bite
α = lubricant pressure-viscosity coefficient or index
δ = depth of the valley
$\varepsilon(\varepsilon_a)$ = bulk (asperity) strain
$\dot{\varepsilon}(\dot{\varepsilon}_a)$ = bulk (asperity) strain rate
$\eta(\eta_0)$ = viscosity of lubricant (at ambient pressure)
θ = pit slope
$\phi, (\phi_0)$ = entraining angle between roll and strip (at inlet)
σ_0 = initial combined R_q roughness of tool and strip
ξ = local co-ordinate giving the distance in the sliding direction from the center of the asperity

Appendix

Details of Lo and Wilson's MPHL Model. This Appendix describes further details of the MPHL model derived by Lo and Wilson [13]. The asperity spacing L is assumed much smaller than the bite length. Therefore, the stretching of the peak and underlying material in the bite is treated as locally uniform. Taking ε_a and ε as the asperity and bulk strain respectively, as shown in Fig. 2, we have

$$AL=A_0L_0e^{\varepsilon_a} \tag{A-1}$$

$$L=L_0e^{\varepsilon}. \tag{A-2}$$

Combining these two equations gives the current contact area

$$A=A_0e^{\varepsilon_a-\varepsilon}. \tag{A-3}$$

The local lubricant flow is assumed as one-dimensional. The local co-ordinates and origin are defined as in Fig. 3. The origin is in the middle of the asperity peak, ξ is a local co-ordinate in the direction of sliding, and h is in the direction perpendicular to the oil film. Considering the stretching speed of the asperity, Lo and Wilson derive the mean oil velocity at the edge of the asperity peak $\overline{u_1}$ as

$$\overline{u_1}=\frac{u_1+\dot{\varepsilon}_a\xi_1}{2}=\frac{u_1-AL\dot{\varepsilon}_a/2}{2}, \tag{A-4}$$

where u_1 is the sliding speed, $\dot{\varepsilon}_a$ is the stretching rate of the peak and ξ_1 is the co-ordinate at the edge of the pit.

During the whole process the pit angle θ is assumed to remain constant so that the oil volume, per unit width, is equal to

$$v=\frac{\theta L^2(1-A)^2}{4}. \tag{A-5}$$

Differentiating this equation with respect to time t gives

$$\frac{dv}{dt}=\frac{\theta L^2(1-A)(\dot{\varepsilon}-A\dot{\varepsilon}_a)}{2}, \tag{A-6}$$

where $\dot{\varepsilon}$ is the strain rate on the underlying material.

The lubricant velocity in the local co-ordinate system is $\overline{u_1}$ while the edge of the "reservoir" is moving at a velocity of $-AL\dot{\varepsilon}_a/2$. Therefore the relative velocity of the lubricant leaving the "reservoir" is $\overline{u_1}+AL\dot{\varepsilon}_a/2$. Assuming the outflow lubricant film thickness is h_1 as shown in Fig. 3, the lubricant flow rate is equal to

$$\frac{dv}{dt} = -h_1\left(\frac{u_1 + AL\dot{\varepsilon}_a/2}{2}\right). \qquad (A\text{-}7)$$

Combining these two equations gives the oil film thickness at the edge of the contact as

$$h_1 = -\frac{2\theta L^2(1-A)(\dot{\varepsilon} - A\dot{\varepsilon}_a)}{2u_1 + AL\dot{\varepsilon}_a}. \qquad (A\text{-}8)$$

References

[1] Sutcliffe, M. P. F., and Johnson, K. L., 1990, ''Lubrication in Cold Strip Rolling in the 'Mixed' Regime,'' Proc. Inst. Mech. Eng., **204**, pp. 249–261.

[2] Sheu, S. and Wilson, W. R. D., 1994, ''Mixed Lubrication of Strip Rolling,'' STLE Tribol. Trans., **37**, pp. 483–493.

[3] Lin, H. S., Marsault, N., and Wilson, W. R. D., 1998, ''A Mixed Lubrication Model for Cold Strip Rolling Part I: Theoretical,'' STLE Tribol. Trans., **41**, pp. 317–326.

[4] Marsault, M., and Montmitonnet, P., Deneuville, P., and Gratacos, P., 1998, ''A Model of Mixed Lubrication for Cold Rolling of Strip,'' Proceedings of NUMIFORM 98: Enschede, Netherlands, June 1998, J. Huétink and F. P. T. Baaijens, eds., A. A. Balkema, Rotterdam, pp.715–720.

[5] Sutcliffe, M. P. F., 1990, ''Surface Asperity Deformation in Metal Forming Processes,'' Int. J. Mech. Sci., **30**, pp. 847–868.

[6] Wilson, W. R. D., and Sheu, S., 1988, ''Real Area of Contact and Boundary Friction in Metal Forming,'' Int. J. Mech. Sci., **30**, pp. 475–489.

[7] Lo, S. W., 1994, ''A Study on the Flow Phenomena in the Mixed Lubrication Regime by Porous Medium Model,'' ASME J. Tribol., **116**, pp. 640–647.

[8] Lo, S. W., 1995, ''Die-Workpiece Interfacial Behaviors in Axisymmetric Forging Processes with Flat Dies,'' STLE Tribol. Trans., **38**, pp. 663–671.

[9] Mizuno, T., and Okamoto, M., 1982, ''Effects of Lubricant Viscosity at Pressure and Sliding Velocity on Lubricating Conditions in the Compression-Friction Test on Sheet Metals,'' J. Lubr. Technol., **104**, pp. 53–59.

[10] Kudo, H., and Azushima, A., 1987, ''Interaction of Surface Microstructure and Lubricant in Metal Forming Tribology,'' *Proc. 2nd Int. Conf. On Adv. Technol. of Plasticity*, Stuttgart, Germany, 373.

[11] Wang, Z., Dohda, K., Yokoi, N., and Haruyama, Y., 1997, ''Outflow Behaviour of Lubricant in Micro Pits in Metal Forming,'' *First International Conference on Tribology in Manufacturing Processes*, Gifu, Japan, pp. 77–82.

[12] Ahmed, R., and Sutcliffe, M. P. F, 2000, ''Identification of Surface Features on Cold Rolled Stainless Steel,'' Wear, **244**, pp. 60–70.

[13] Lo, S. W., and Wilson, W. R. D., 1999, ''A Theoretical Model of Micro-pool Lubrication in Metal Forming,'' ASME J. Tribol., **121**, pp. 731–738.

[14] Sheu, S., Hector, L. G., Karabin, M. E., 1999, ''Two-Scale Surface Topography Design Scheme for Friction and Wear Control in Forging: Theory and Experiment,'' *The Integration of Material Process and Product Design*, Zabaras et al., eds., AA Balkema, Rotterdam, pp. 157–166.

[15] Sutcliffe, M. P. F., 1999, ''Flattening of Random Rough Surfaces in Metal Forming Processes,'' ASME J. Tribol., **121**, pp. 433–440.

[16] Korzekwa, D. A., Dawson, P. R., and Wilson, W. R. D, 1992, ''Surface Asperity Deformation During Sheet Forming,'' Int. J. Mech. Sci., **34**, pp. 521–539.

[17] Ahmed, R., and Sutcliffe, M. P. F., 2001, ''An Experimental Investigation of Surface Pit Evolution During Cold-Rolling or Drawing of Stainless Steel Strip,'' ASME J. Tribol., **123**, pp. 1–7.

[18] Wilson, W. R. D., and Walowit, J. A., 1972, ''An Isothermal Hydrodynamic Lubrication Theory for strip Rolling with Front and Back Tension,'' *Tribology Convention*, IMechE, London, pp. 164–172.